

A Tensor-Train Decomposition based Compression of LLMs on Group Vector Systolic Accelerator

Sixiao Huang, Tintin Wang, Ang Li, Ao Shen, Kai Li, Keyao Jiang, Mingqiang Huang and Hao Yu

Abstract—Large language models (LLMs) are both storage-intensive and computation-intensive, posing significant challenges when deployed on resource-constrained hardware. As linear layers in LLMs are mainly resource consuming parts, this paper develops a tensor-train decomposition (TTD) for LLMs with a further hardware implementation on FPGA. TTD compression is applied to the linear layers in ChatGLM3-6B and LLaMA2-7B models with compression ratios (CRs) for the whole network $1.94\times$ and $1.60\times$, respectively. The compressed LLMs are further implemented on FPGA hardware within a highly efficient group vector systolic array (GVSA) architecture, which has DSP-shared parallel vector PEs for TTD inference, as well as optimized data communication in the accelerator. Experimental results show that the corresponding TTD based LLM accelerator implemented on FPGA achieves $1.45\times$ and $1.57\times$ reduction in first token delay for ChatGLM3-6B and LLaMA2-7B models, respectively.

Index Terms—Tensor-Train Decomposition, Linear Layer, Systolic Array, FPGA, LLM.

I. INTRODUCTION

Artificial intelligence has already demonstrated extraordinary accuracy across numerous tasks, profoundly impacting people’s lives [1]–[4]. However, deploying deep neural networks (DNNs) on edge devices is very challenging due to limited storage, computing resources, and power consumption. Previous work [5]–[8] has focused on accelerating convolutional neural networks (CNNs), primarily optimizing convolutional layers inference, while linear layers are converted to convolutional computations. However, due to the low ratio of operations to weight number of linear layers, the memory access limits for performance of accelerators, as described by the “Roofline” model [9]. Transformers and LLMs are developing rapidly, most of whose computation are linear layers. Therefore, solving the issue of large memory access in linear layers is crucial for deploying LLMs on edge devices with efficient performance.

There are two primary approaches for compressing DNNs to decrease the memory access. The first approach is reducing the bit width of data, known as quantization [10], [11]. This method converts the neural network weights into integer numbers, which consume fewer bits than the full-precision floating-point values used during network training. This not only reduces the size of the weights but also makes network computations more hardware-friendly, as the integer calculations require significantly fewer hardware resources and power compared to floating-point calculations. Previous work [12] deployed NAS optimized multi-precision CNN models on FPGA and achieved impressive results. The second approach focuses on reducing the number of weights through techniques

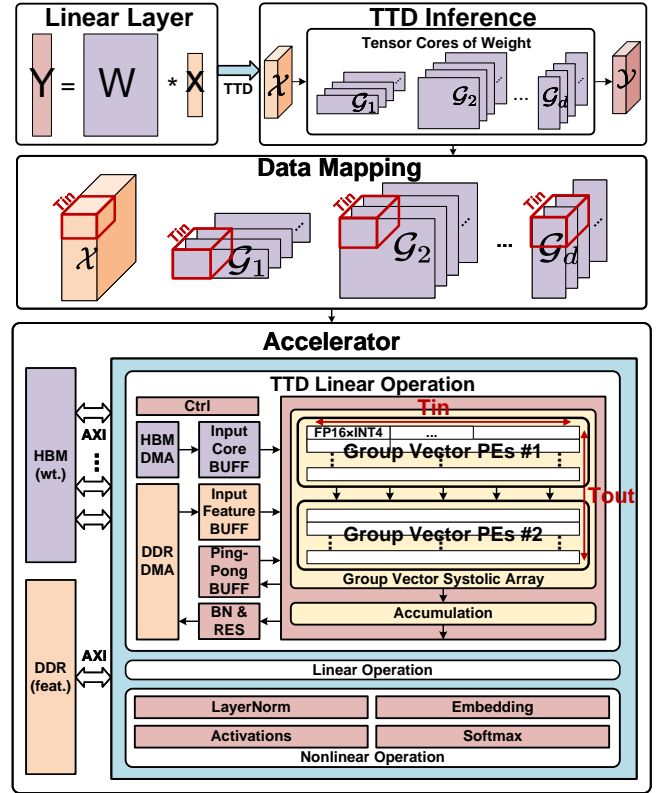


Fig. 1. LLMs with TTD compressed linear layers mapping on FPGA implemented group vector systolic accelerator.

such as sparse pruning [13] and low-rank compression. These methods decrease the number of weights by changing the network’s architecture. Among these compression methods, low-rank compression stands out due to its high compression ratio (CR), especially the tensor-train decomposition (TTD) method [14]. Experiments have shown that applying TTD to the linear layers of VGG16 on the ImageNet dataset achieved a CR of $50,000\times$ [15]. Previous works [16]–[18] show that TTD performs effectively on RNNs and 3D point cloud models. Despite TTD’s remarkable compression capabilities, it changes the computational structure of linear layers, necessitating a redesign of hardware to accelerate efficiently.

In this paper, we propose an FPGA-based accelerator to accelerate TTD compressed LLMs which is shown in Fig. 1. First, TTD compression is applied to linear layers in ChatGLM3-6B and LLaMA2-7B with whole-network CRs of $1.94\times$ and $1.60\times$, respectively. Second, we implement the TTD inference of the linear layer on hardware. Not only do we

need to reduce the redundant computation and memory access in the original TTD inference, but we also need to perform the reordering operation on the intermediate data during the TTD. To achieve optimize hardware efficiency, the accelerator uses a group vector systolic array (GVSA) to perform matrix computations during TTD inference. The DSP-shared parallel vector processing elements (PEs) execute FP16 and INT4 multiply-accumulate (MAC) operations. Through operator fusion, we implement three operations on the accelerator: TTD linear operation, linear operation, and nonlinear operation. By configuring and chaining these operations together, edge deployment of TTD compressed LLMs can be achieved. Finally, we implement the accelerator design on the AMD Alveo V80 FPGA to deploy ChatGLM3-6B and LLaMA2-7B after TTD compression. Compared to the baseline without the TTD inference, the accelerator achieves $1.45\times$ and $1.57\times$ reduction in first token delay for ChatGLM3-6B and LLaMA2-7B, respectively.

II. TTD COMPRESSED LINEAR LAYER

A. Linear Layers in LLMs

Fig. 2 shows the architecture of ChatGLM3-6B [19] and LLaMA2-7B [20], which consists of word embedding, transformer blocks, and output layers. The transformer blocks are composed of multiple repeated blocks in sequence. A single block is made up of a multi-head attention (MHA) and a multilayer perceptron (MLP). The MHA consists of linear layers, matrix multiplication, and softmax, while the MLP is composed of linear layers and activation functions. It is evident that most of the computations in LLMs are linear layer operations. Therefore, to deploy LLMs on edge devices efficiently, it is essential to compress the linear layers to reduce the number of network weights.

B. Tensorization

The weights of the linear layers described in the previous section are all two-dimensional matrices, whereas the TTD algorithm is applied to higher-dimensional tensor (dimension greater than 2). Therefore, to apply TTD to compress the weight matrix of the linear layer, it first needs to be tensorized. Tensorization is the process of converting low-dimension data (vector or matrix) into high-dimension data (tensor). For example, there is a matrix $T \in \mathbb{R}^{M_1 \times M_2}$, and its tensorized form is $\mathcal{T} \in \mathbb{R}^{v_1 \times v_2 \times \dots \times v_d}$ which is a d -dimensional tensor. The number of elements remains the same before and after tensorization. So $M_1 M_2 = \prod_{i=1}^d v_i$. Through this process, the weight matrix of the linear layer can be transformed into a tensor of arbitrary dimensions, facilitating the subsequent application of TTD.

C. Tensor-Train Decomposition

TTD [14] has been proved for compressing multi-dimensional tensors into a more compact form. This method decomposes a high-dimensional tensor into a sequence of

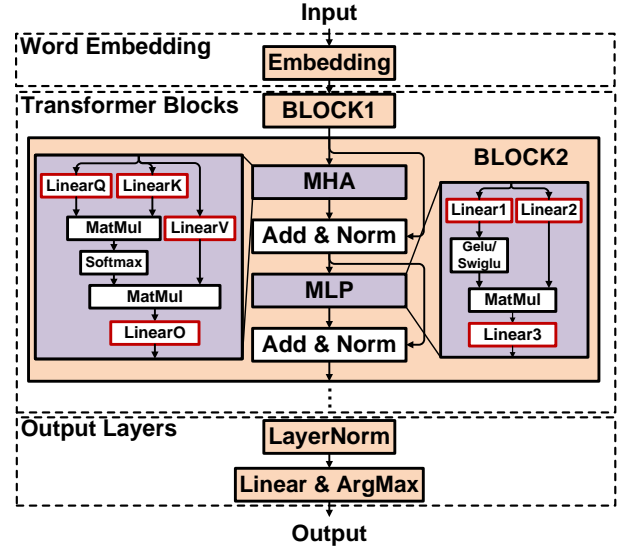


Fig. 2. Architecture of ChatGLM3-6B and LLaMA2-7B.

lower-dimensional tensors, known as cores, which are multiplied together in a specific order. Specifically, for a d -dimensional tensor $\mathcal{T} \in \mathbb{R}^{v_1 \times v_2 \times \dots \times v_d}$, it can be decomposed as follows:

$$\mathcal{T}(l_1, \dots, l_d) = \mathcal{G}_1[l_1] \mathcal{G}_2[l_2] \dots \mathcal{G}_d[l_d] \quad (1)$$

where $\mathcal{G}_k[l_k] \in \mathbb{R}^{r_{k-1} \times r_k}$ is the l_k slice of the k^{th} core \mathcal{G}_k and $l_k \in [1, v_k]$ and r_k is the rank. To satisfy the shape of the tensor, r_0 and r_d are set as 1. And the CR of TTD is:

$$CR = \frac{\prod_{k=1}^d v_k}{\sum_{k=1}^d v_k r_{k-1} r_k} \quad (2)$$

where the ranks of cores are always small, so the compression effect will be very obvious. The basic principle of tensorization and TTD is shown in Fig. 3.

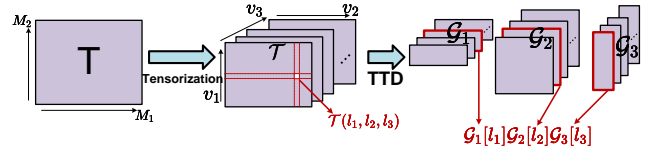


Fig. 3. Basic principles of tensorization and TTD (Example with $d = 3$).

D. TTD Compression and Inference

We can perform a TTD compressed linear layers for inference as shown in Algorithm 1 below. The linear layer can be simply expressed as $Y = Wx$ where $Y \in \mathbb{R}^M$, $W \in \mathbb{R}^{M \times N}$ and $x \in \mathbb{R}^N$. First, we need to perform tensorization operations on the input and weight matrices to tensor $\mathcal{W} \in \mathbb{R}^{(m_1 \times n_1) \times \dots \times (m_d \times n_d)}$ and $\mathcal{X} \in \mathbb{R}^{n_1 \times \dots \times n_d}$ where $M = \prod_{k=1}^d m_k$ and $N = \prod_{k=1}^d n_k$. Note that here, d corresponds to the number of cores \mathcal{G} generated by TTD later. Additionally, we need to determine the rank of the cores for TTD, which affects the CR of TTD and the similarity between the reconstructed matrix from the cores and the original weight matrix. A higher rank results in a lower CR and higher

Algorithm 1 TTD compression of linear layers

Input: The input and weight of the linear layer, x, W ; The dimension number of TTD, d ; The rank of TTD, r .

Output: The input and cores of TTD compressed linear layer, $\mathcal{X}, \mathcal{G}_1, \dots, \mathcal{G}_d$.

```

1:  $n_1, n_2, \dots, n_d = \text{Factorization}(N, d)$ 
2:  $m_1, m_2, \dots, m_d = \text{Factorization}(M, d)$ 
3:  $\mathcal{X} = \text{Tensorization}(x, (n_1, \dots, n_d))$ 
4:  $\mathcal{W} = \text{Tensorization}(w, (n_1 m_1, \dots, n_d m_d))$ 
5:  $\mathcal{G}_1, \mathcal{G}_2, \dots, \mathcal{G}_d = \text{TTD}(\mathcal{W}, (n_1 m_1, \dots, n_d m_d), r)$ 
6: return  $\mathcal{X}, \mathcal{G}_1, \mathcal{G}_2, \dots, \mathcal{G}_d$ 
7: function TTD( $\mathcal{W}, (n_1 m_1, \dots, n_d m_d), r$ ) [14]
8:   Initialization
9:   Temporary tensor:  $C = \mathcal{W}, r_0 = 1$ ;
10:  for each  $k \in [1, d - 1]$  do
11:     $C = \text{reshape}(C, [r_{k-1} n_k m_k, \frac{\text{numel}(C)}{r_{k-1} n_k m_k}])$ 
12:    Compute SVD:  $C = USV + E$ 
13:    New core:  $\mathcal{G}_k = \text{reshape}(U, [r_{k-1}, n_k m_k, r_k])$ 
14:     $C = SV^T$ 
15:  end for
16:   $\mathcal{G}_d = C$ 
17:  return  $\mathcal{G}_1, \dots, \mathcal{G}_d$ 
18: end function
  
```

similarity and it has a smaller impact on network accuracy. The TTD inference of linear layers can be expressed as:

$$\mathcal{Y}(j_1, \dots, j_d) = \sum_{i_1 \dots i_d} \mathcal{G}_1[i_1, j_1] \mathcal{G}_2[i_2, j_2] \dots \mathcal{G}_d[i_d, j_d] \mathcal{X}(i_1, \dots, i_d) \quad (3)$$

where the output $\mathcal{Y} \in \mathbb{R}^{m_1 \times m_2 \times \dots \times m_d}$ is the high-dimension tensor format of Y after TTD. And $\mathcal{G}_k \in \mathbb{R}^{m_k \times r_{k-1} \times r_k \times n_k}$ is k^{th} core of weight tensor \mathcal{W} .

By compressing the weight matrix of the linear layer using TTD, we obtain the corresponding cores. The TTD inference of the linear layer can be performed as described in Equation (3). This involves multiplying the tensorized input by the cores of weights of TTD compressed linear layer, and then summing over all input dimensions i_k to obtain the final tensorized output.

III. TTD INFERENCE OF LLMs ON GVSA

A. Operator Fusion of LLMs Inference

For various operations in the LLMs inference process such as linear layers, batch normalization (BN) and residual connections (Res), operator fusion can be applied to merge two adjacent operators, reducing redundant data transfers, between off-chip and on-chip memory, thereby improving throughput.

Through operator fusion, the inference of TTD compressed LLMs is achieved by configuring three main operations in the accelerator: TTD linear operation, linear operation and nonlinear operation. The TTD linear operation focuses on TTD inference for the linear layer, integrating BN and Res operations. The linear operation handles the regular linear layer and related operations. The nonlinear operation is responsible for

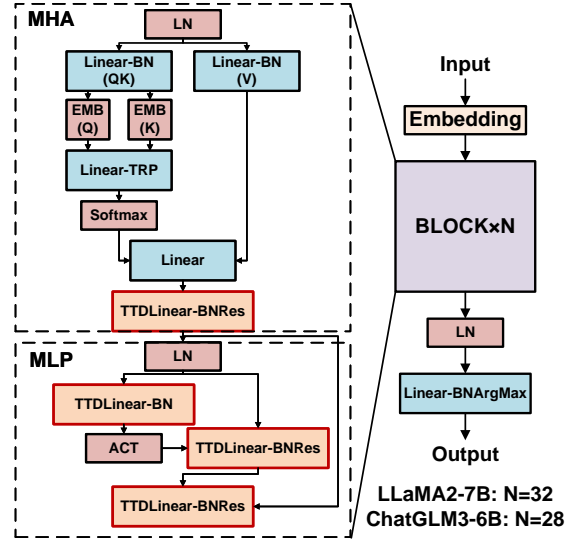


Fig. 4. Operator execution order for inference of TTD compressed LLMs.

various nonlinear operations, such as layer normalization (LN), embedding (EMB), activation functions (ACT) and softmax. Fig. 4 shows the operators execution order for the inference of ChatGLM3-6B and LLaMA2-7B after TTD compression.

The compiler generates serialized instructions based on the network architecture. These instructions configure operations by writing to registers, including the information of operations and the addresses of input and output data in HBM/DDR. The serialized instructions ensure the sequential chaining of operations and completing the inference of the entire network.

B. GVSA Architecture

We utilize the GVSA architecture in [21] employing a multiple row-by-row systolic computing style to achieve the highly efficient matrix multiplication as shown in Fig. 5. The array consists of T_{out} PEs, each performing T_{in} MAC operations. Parallel computation with T_n PEs, executes MAC operations for $1 \times T_{in}$ feature with $T_n \times T_{in}$ weight. At each cycle, only one weight vector is loaded into this array. Meanwhile, all of others remain stationary within the PEs for T_{out} cycles until they are replaced by a new one. Feature vectors are sequentially fed into the array and passed from one group of parallel vector PEs to the next.

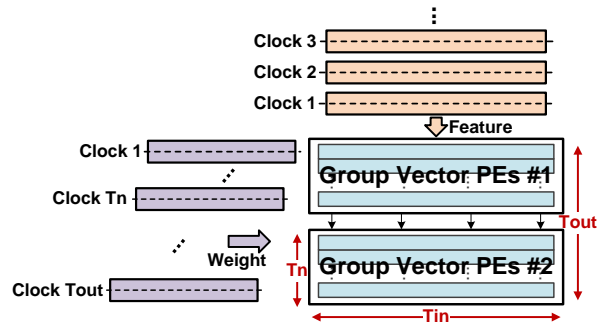


Fig. 5. Architecture of GVSA when $T_n = T_{out}/2$.

C. TTD Inference Data Mapping on GVSA

For TTD inference, as shown in Equation (3), if the computation is performed by multiplying cores by the input and then accumulating the input dimensions i_k to obtain the final output, it will result in a lot of unnecessary memory access and computation. For example, in a 4-dimensional TTD inference, consider two output results $\mathcal{Y}(j_1, j_2, j_3, j_4)$ when their $j_1, j_2, j_3 = 0$ and one $j_4 = 1$, while the other $j_4 = 2$. If you need to calculate these two values, their cores $\mathcal{G}_1, \mathcal{G}_2, \mathcal{G}_3$ are all the same due to the same value of output dimension in j_1, j_2, j_3 , and only cores \mathcal{G}_4 are different. Thus, the computation of the partial products and memory access for the first three cores is redundant. Therefore, a more efficient computation strategy becomes necessary.

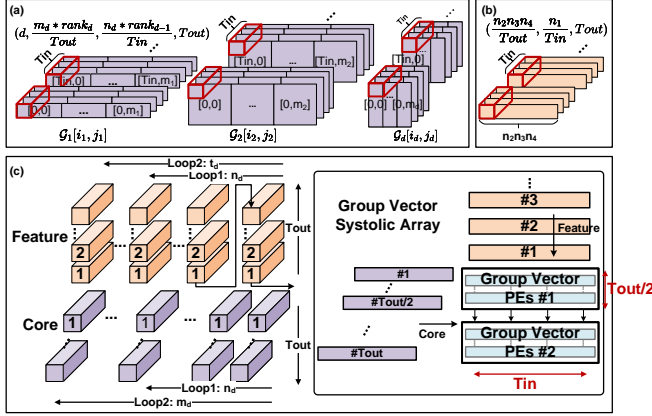


Fig. 6. (a) Data mapping of cores; (b) Data mapping of input features; (c) Operation stages on GVSA for TTD inference.

We first split the computation order, starting with the first input dimension i_1 and proceeding sequentially until summing over the final input dimension i_d . In this computation order, assuming we denote the partial computation results as \mathcal{P} , each layer's calculation involves multiplying the last partial result \mathcal{P}_{k-1} with the current core \mathcal{G}_k and then summing over the input dimension i_k , as shown in Equation (4).

$$\overline{\mathcal{P}}_k[t_{k-1}, j_k] = \sum_{i_k} \mathcal{G}_k[i_k, j_k] \mathcal{P}_{k-1}[i_k, t_{k-1}] \quad (4)$$

where $\mathcal{P}_0 = \mathcal{X}$, and $\overline{\mathcal{P}}_d = \mathcal{Y}$. And $\overline{\mathcal{P}}_k[t_{k-1}, j_k]$ is reordered to $\mathcal{P}_k[i_k, t_k]$. t_k is the other dimension of stage k , such as, $t_0 = [i_2, i_3, i_4]$ (example with $d=4$) and $t_1 = [i_3, i_4, j_1]$. The following part will introduce the data mapping and data flow of the accelerator when executing TTD inference of linear layer.

Data Preparation Stage. The input \mathcal{X} and weight cores \mathcal{G} are input to the accelerator from the off-chip DDR and HBM through the AXI bus, and the DMA stores them in the buffer.

Stage 1. When the data is prepared for computation, it is processed in Stage 1 (S1), characterized by a multi-level loop calculation within GVSA. For the data flow of \mathcal{X} into GVSA, where i_1 is the summation dimension and its parallelism is T_{in} , it will first complete the loop over T_{out} on output dimension, and then complete the loop over the summation dimension

which is $\lceil n_1/T_{in} \rceil$. Finally, it completes the loops over other dimensions which is $\lceil (n_2 \times n_3 \times n_4)/T_{out} \rceil$. For the TTD core \mathcal{G}_1 , the process is similar: first, loop over T_{out} , then complete the loop of the summation dimension, and finally loop over the output dimension which is $\lceil (m_1 \times \text{rank})/T_{out} \rceil$. In S1, the control unit reads the input feature \mathcal{X} and \mathcal{G}_1 core data from the input buffer. The output $\overline{\mathcal{P}}_1$ is written into the ping-pong buffers. The shape of the cores and input feature and operation scheme with GVSA are shown in Fig. 6.

Stage 2. Next, in Stage 2 (S2), the loops for the \mathcal{G}_2 core are similar to those in S1, with the exception that the summation dimension loop is $\lceil (n_2 \times \text{rank})/T_{in} \rceil$. The input \mathcal{P}_1 undergoes reordering. In this process, since the summation dimension i_2 in S2 is positioned within the output dimension (i_2, i_3, i_4, j_1) of $\overline{\mathcal{P}}_1$ and it repeats in the time direction for each T_{out} cycle, it must be extracted and reconstituted into \mathcal{P}_1 with T_{in} parallelism to match the input format of GVSA. This reordering operation is embedded within the writing of $\overline{\mathcal{P}}_1$ and the reading of \mathcal{P}_1 .

The remaining stages are similar until all stages are completed. The results are input to BN and Res modules and then written to the external DDR by DMA.

Reorder Between Stages. We reorder $\overline{\mathcal{P}}_1$ to \mathcal{P}_1 by writing the T_{out} -length vector-shaped output of S1 to the ping-pong buffers which has two dimensions: block dimension which is summation dimension in S2 and address dimension which is the time dimension in S2. In S2, the parts of the input \mathcal{P}_1 are read from the same address across different blocks of buffers. By such operations, the reordering process is hidden in the reading and writing of intermediate data between stages in the ping-pong buffers, avoiding the waiting time and eliminating the need for a reordering unit.

IV. FPGA IMPLEMENTATION

The architecture of the TTD linear operation in the accelerator as shown in the Fig. 1 comprises DDR/HBM Direct Memory Access (DMA), an input buffer, ping-pong buffers, a GVSA and a control unit. The DMA is responsible for transferring input features and cores of TTD from external DDR and HBM to the on-chip buffer, as well as moving the output data to the DDR. The ping-pong buffers store intermediate data in every stage of TTD inference. The control unit manages the reading and writing data from the buffers.

Because of the complex structure and various operations, efficiently utilizing limited resources is essential when deploying LLMs on FPGA. We propose DSP-shared floating-point parallel vector PEs to execute $\text{FP16} \times \text{INT4}$ operations, which not only adapts to the data flow of the GVSA but also optimizes the utilization of DSP resources. As shown in Fig. 7(b), the multipliers in the DSPs on the Xilinx Ultrascale+ platform have input bit widths of 27 and 18. Previous works [22]–[24] have used DSPs for various integer calculations. By a similar approach, we can achieve $\text{FP16} \times \text{INT4}$ computations through the arrangement of input data.

The FP16 format consists of a 1-bit sign, a 5-bit exponent, and a 10-bit mantissa. To perform FP16 and INT4 multi-

TABLE I
INFORMATION OF EVALUATED BENCHMARKS FOR THE ACCELERATOR

Benchmark	Operations	Size	n	m	Rank	Precision	CR for	CR for	CR for	Score Decrease	PPL Increase
							Linear Layer	Single Block	Whole Network		
ChatGLM3-6B Block	MHA	LinearQ	4096×4096	-	-	-	1	10.72	1.94	4.21	-
		LinearK	4096×256	-	-	-	1				
		LinearV	4096×256	-	-	-	1				
		LinearO	4096×4096	[16,8,8,4]	[4,8,8,16]	16	481.88				
	MLP	Linear1	4096×13696	[8,8,8,8]	[4,4,8,107]	16	1446.44				
		Linear2	4096×13696	[8,8,8,8]	[4,4,8,107]	16	1446.44				
Linear3		13696×4096	[107,8,4,4]	[8,8,8,8]	16	1446.44					
LLaMA2-7B Block	MHA	LinearQ	4096×4096	-	-	-	1	4.01	1.60	-	2.62
		LinearK	4096×4096	-	-	-	1				
		LinearV	4096×4096	-	-	-	1				
		LinearO	4096×4096	[16,8,8,4]	[4,8,8,16]	16	481.88				
	MLP	Linear1	4096×11008	[16,8,8,4]	[4,4,16,43]	16	1233.82				
		Linear2	4096×11008	[16,8,8,4]	[4,4,16,43]	16	1233.82				
Linear3		11008×4096	[43,16,4,4]	[4,8,8,16]	16	1007.89					

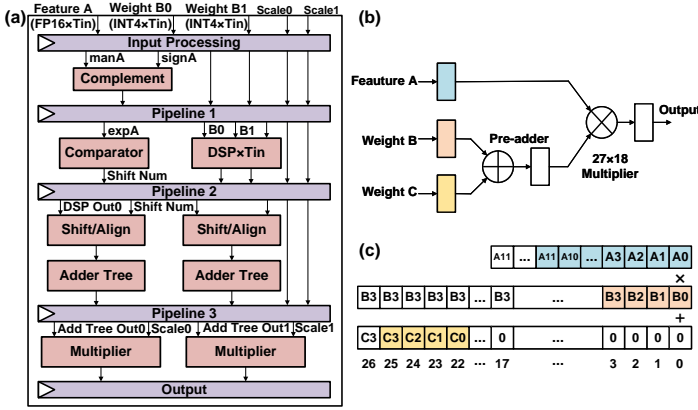


Fig. 7. (a)DSP-shared GVSA vector PEs; (b)According design by DSP in Xilinx; (c) Data arrangement of DSP inputs.

plication, we need to multiply the signed 4-bit fixed-point number by the 12-bit two’s complement representation of $\{sign, hiddenbit, mantissa\}$. As mentioned above, the adequate input bit width of the DSP allows us to simultaneously perform multiplication of a two’s complement mantissa and two INT4 weights. The arrangement of DSP inputs is shown in Fig. 7(c). In this way, the output of the DSP includes two 16-bit multiplication results. Through this DSP-shared strategy, we not only meet the data flow requirements of GVSA but also save DSP resources. By using multiple such PEs in parallel externally, we can achieve various levels of parallelism.

For the DSP-shared vector PEs, due to the multiple steps in floating-point calculations, we design it in a pipeline structure shown in Fig. 7(a). One feature vector and two weight vectors are fed into the vector PEs. First, the parts of the FP16 format are separated, and the $\{sign, hiddenbit, mantissa\}$ data passes a two’s complement operation. Next, the 12-bit two’s complement and the fixed-point weight data are fed into the DSPs. Simultaneously, the floating-point exponent bits are compared to determine the shift amount relative to the maximum exponent bit for subsequent adder trees. The DSP output is then shifted according to the determined shift amount and fed into the adder trees. In the final pipeline stage, the input scale is multiplied with the result of the accumulation.

V. EXPERIMENTAL RESULTS

A. Experiment Setup

We used Vivado 2024.1 software to synthesize and implement our proposed accelerator on the AMD Alveo V80 FPGA platform with 12574K LUTs, 5148K FFs, 3741 Block RAMs (BRAMs) and 10848 DSPs. This FPGA integrates 32GB of HBM which is suitable for LLMs inference.

The benchmarks for this accelerator are TTD compressed ChatGLM3-6B and LLaMA2-7B. To ensure the accuracy of these networks, we choose specific blocks to perform TTD compression and INT4 quantization on the linear layers excluding $Attention(Q, K, V)$, while the remaining parts perform only INT4 quantization. These TTD compressed blocks are concatenated with the other quantized blocks and quantized output layers to construct the final deployed network. The configurations of the benchmarks are shown in the Table I.

In deploying the inference process of TTD compressed LLMs, the operators of the accelerator are deployed and executed sequentially according to the operator chaining order in Fig. 4, completing the accelerator system emulation for V80 on the benchmarks which is similar with the experiment setup of FlightLLM [25].

TABLE II
RESOURCE UTILIZATION OF THE ACCELERATOR ON V80

Resource	Available	TTD Linear Operation	Other Operations	Total
LUT	2574K	403K(15.68%)	903K	1307K(50.79%)
FF	5148K	349K(6.78%)	569K	919K(17.85%)
BRAM	3741	643(17.19%)	447	1090(29.14%)
DSP	10848	2159(19.90%)	7286	9445(87.07%)

B. Network Performance Evaluation

The CRs and performance of TTD compressed LLMs are shown in Table I. The number of TTD compressed blocks of ChatGLM3-6B and LLaMA2-7B is 15 and 19, respectively. The TTD compression for ChatGLM3-6B and LLaMA2-7B achieves $481.88\sim 1446.44\times$ CRs for linear layers, $10.72\times$ and $4.01\times$ CRs for single block, $1.94\times$ and $1.60\times$ CRs for whole network, respectively. Compared to the original model, the average score on C-Eval tests [26] of ChatGLM3-6B after TTD compression and quantization shows a decrease of 4.21. The perplexity (PPL) on C4 dataset [27] of LLaMA2-7B shows an increase of 2.62.

TABLE III
TTD COMPRESSED CHATGLM3-6B ON V80

ChatGLM3-6B	Operations	Delay(us)	
Block	MHA	LN	11.39
		Linear-BN(QK)	51.03
		EMB(Q)	6.54
		EMB(K)	6.80
		Linear-TRP	8.24
		Softmax	26.08
		Linear-BN(V)	7.47
	MLP	Linear	8.99
		TTDLinear-BNRes	29.32
		LN	11.63
		TTDLinear-BN	43.04
		ACT	21.87
		TTDLinear-BNRes	43.49
		TTDLinear-BNRes	37.22
Output Layer	LN	13.78	
	Linear-BNArgmax	701.18	
Summary	First token delay: 14.34ms Peak speed: 69.7token/s(1.45×)		

TABLE IV
TTD COMPRESSED LLAMA2-7B ON V80

LLaMA2-7B	Operations	Delay(us)	
Block	MHA	LN	12.57
		Linear-BN(QK)	91.23
		EMB(Q)	4.82
		EMB(K)	6.80
		Linear-TRP	47.35
		Softmax	22.35
		Linear-BN(V)	51.94
	MLP	Linear	44.13
		TTDLinear-BNRes	29.34
		LN	11.00
		TTDLinear-BN	27.03
		ACT	12.43
		TTDLinear-BNRes	27.74
		TTDLinear-BNRes	24.73
Output Layer	LN	12.28	
	Linear-BNArgmax	349.16	
Summary	First token delay: 15.20ms Peak speed: 65.8token/s(1.57×)		

C. Hardware Performance Evaluation

For GVSA in the TTD linear operation, T_{in} , T_{out} and T_n are set to 128, 32 and 16, respectively. The frequency of system operation of this accelerator is set at 125MHz. The resource utilization is shown in Table II. The deployment of the ChatGLM3-6B and LLaMA2-7B on the accelerator is shown in Table III and Table IV, respectively. For this accelerator, we map the inference process of single block in ChatGLM3-6B and LLaMA2-7B into a 14 steps of operators, and output layers mapped into 2 steps. We also use a same accelerator but without TTD inference as a baseline. As shown in Fig. 8, the accelerator achieves $3.22\times$ and $3.88\times$ speedup in the MLP inference, $2.19\times$ and $1.78\times$ speedup in the single block inference and $1.45\times$ and $1.57\times$ reduction in the first token delay of ChatGLM3-6B and LLaMA2-7B, respectively.

Fig. 9(a) shows the speed of the accelerator when executing ChatGLM3-6B and LLaMA2-7B for different number of decoded tokens. It can be seen that the KV cache strategy mitigates the decrease in speed when generating longer statements and the accelerator with TTD inference always has better performance than the baseline. Fig. 9(b) shows the normalized throughput of the accelerator compared to

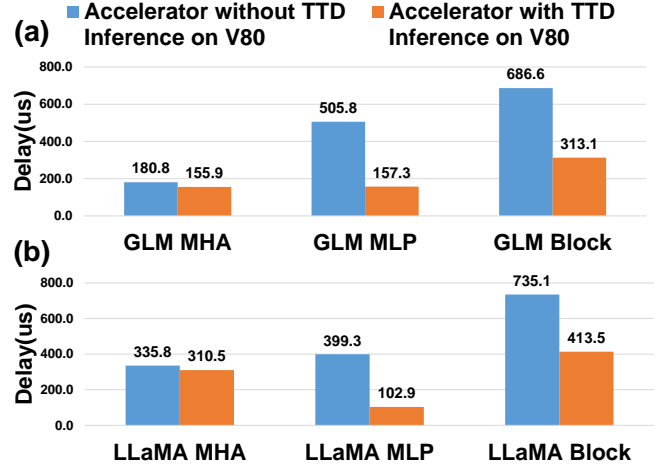


Fig. 8. Performance comparison with accelerator without TTD inference on (a) ChatGLM3-6B and (b) LLaMA2-7B.

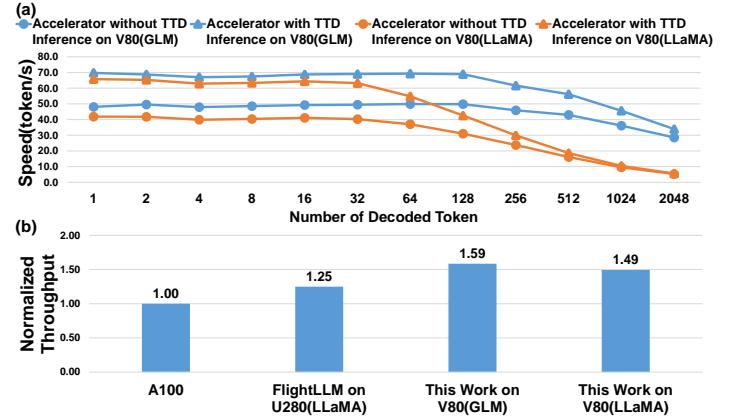


Fig. 9. (a) Speed comparison with accelerator without TTD inference at different token number in decoding stage of ChatGLM3-6B and LLaMA2-7B. (b) Normalized throughput comparison with different hardware platform.

other hardware platforms. The accelerator with TTD inference achieves 59% and 49% higher throughput compared to the A100 GPU. FlightLLM is a current advanced LLM accelerator that achieves good throughput through sparsity and mixed precision. By applying TTD compression to LLMs, optimizing the data flow of TTD inference and using highly efficient GVSA, our accelerator achieves a 27% and 19% higher throughput compared to FlightLLM on U280.

VI. CONCLUSION

In this paper, we implement TTD compressed LLMs and deploy their inference on FPGA. The TTD inference is mapped onto a highly efficient GVSA with DSP-shared parallel vector PEs. Experimental results show that the proposed accelerator achieves a $3.22\times$ and $3.88\times$ speedup in the MLP inference, $2.19\times$ and $1.78\times$ speedup in the single block inference and $1.45\times$ and $1.57\times$ reduction in first token delay on ChatGLM3-6B and LLaMA2-7B, respectively.

REFERENCES

- [1] O. Russakovsky, J. Deng, H. Su, J. Krause, S. Satheesh, S. Ma, Z. Huang, A. Karpathy, A. Khosla, M. Bernstein *et al.*, “Imagenet large scale visual recognition challenge,” *International journal of computer vision*, vol. 115, pp. 211–252, 2015.
- [2] J. Long, E. Shelhamer, and T. Darrell, “Fully convolutional networks for semantic segmentation,” in *Proceedings of the IEEE conference on computer vision and pattern recognition*, 2015, pp. 3431–3440.
- [3] G. Hinton, L. Deng, D. Yu, G. E. Dahl, A.-r. Mohamed, N. Jaitly, A. Senior, V. Vanhoucke, P. Nguyen, T. N. Sainath *et al.*, “Deep neural networks for acoustic modeling in speech recognition: The shared views of four research groups,” *IEEE Signal processing magazine*, vol. 29, no. 6, pp. 82–97, 2012.
- [4] A. Vaswani, N. Shazeer, N. Parmar, J. Uszkoreit, L. Jones, A. N. Gomez, L. Kaiser, and I. Polosukhin, “Attention is all you need,” *Advances in neural information processing systems*, vol. 30, 2017.
- [5] M. Huang, Y. Liu, C. Man, K. Li, Q. Cheng, W. Mao, and H. Yu, “A high performance multi-bit-width booth vector systolic accelerator for nas optimized deep learning neural networks,” *IEEE Transactions on Circuits and Systems I: Regular Papers*, vol. 69, no. 9, pp. 3619–3631, 2022.
- [6] Y.-H. Chen, J. Emer, and V. Sze, “Eyeriss: A spatial architecture for energy-efficient dataflow for convolutional neural networks,” *ACM SIGARCH computer architecture news*, vol. 44, no. 3, pp. 367–379, 2016.
- [7] M. Huang, Y. Liu, Q. Cheng, S. Yang, K. Li, J. Luo, Z. Yang, Q. Li, H. Yu, and C. Man, “A high throughput multi-bit-width 3d systolic accelerator for nas optimized deep neural networks on fpga,” in *Proceedings of the 2022 ACM/SIGDA International Symposium on Field-Programmable Gate Arrays*, 2022, pp. 50–50.
- [8] S. Yang, C. Ding, M. Huang, K. Li, C. Li, Z. Wei, S. Huang, J. Dong, L. Zhang, and H. Yu, “Lamps: A layer-wised mixed-precision-and-sparsity accelerator for nas-optimized cnns on fpga,” in *2024 IEEE 32nd Annual International Symposium on Field-Programmable Custom Computing Machines (FCCM)*. IEEE, 2024, pp. 90–96.
- [9] C. Zhang, P. Li, G. Sun, Y. Guan, B. Xiao, and J. Cong, “Optimizing fpga-based accelerator design for deep convolutional neural networks,” in *Proceedings of the 2015 ACM/SIGDA international symposium on field-programmable gate arrays*, 2015, pp. 161–170.
- [10] S.-E. Chang, Y. Li, M. Sun, R. Shi, H. K.-H. So, X. Qian, Y. Wang, and X. Lin, “Mix and match: A novel fpga-centric deep neural network quantization framework,” in *2021 IEEE International Symposium on High-Performance Computer Architecture (HPCA)*. IEEE, 2021, pp. 208–220.
- [11] Z. Guan, H. Huang, Y. Su, H. Huang, N. Wong, and H. Yu, “APTQ: Attention-aware post-training mixed-precision quantization for large language models,” in *Proceedings of the 61st ACM/IEEE Design Automation Conference*, ser. DAC ’24. New York, NY, USA: Association for Computing Machinery, 2024. [Online]. Available: <https://doi.org/10.1145/3649329.3658498>
- [12] Z. He, A. Shen, Q. Li, Q. Cheng, and H. Yu, “Agile hardware and software co-design for risc-v-based multi-precision deep learning microprocessor,” in *Proceedings of the 28th Asia and South Pacific Design Automation Conference*, 2023, pp. 490–495.
- [13] Y. Liang, L. Lu, and J. Xie, “Omni: A framework for integrating hardware and software optimizations for sparse cnns,” *IEEE Transactions on Computer-Aided Design of Integrated Circuits and Systems*, vol. 40, no. 8, pp. 1648–1661, 2020.
- [14] I. V. Oseledets, “Tensor-train decomposition,” *SIAM Journal on Scientific Computing*, vol. 33, no. 5, pp. 2295–2317, 2011.
- [15] A. Novikov, D. Podoprikin, A. Osokin, and D. P. Vetrov, “Tensorizing neural networks,” *Advances in neural information processing systems*, vol. 28, 2015.
- [16] C. Man, C. Chang, C. Ding, A. Shen, H. Ren, Z. Guan, Y. Cheng, S. Luo, R. Zhang, N. Wong *et al.*, “Ranksearch: An automatic rank search towards optimal tensor compression for video lstm networks on edge,” in *2023 Design, Automation & Test in Europe Conference & Exhibition (DATE)*. IEEE, 2023, pp. 1–2.
- [17] Y. Cheng, G. Li, N. Wong, H.-B. Chen, and H. Yu, “Deepeye: A deeply tensor-compressed neural network hardware accelerator,” in *2019 IEEE/ACM International Conference on Computer-Aided Design (ICCAD)*. IEEE, 2019, pp. 1–8.
- [18] Z. Wei, T. Wang, C. Ding, B. Wang, Z. Guan, H. Huang, and H. Yu, “Fmmt: Fused multi-head transformer with tensor-compression for 3d point clouds detection on edge devices,” in *2024 Design, Automation & Test in Europe Conference & Exhibition (DATE)*. IEEE, 2024, pp. 1–6.
- [19] Z. Du, Y. Qian, X. Liu, M. Ding, J. Qiu, Z. Yang, and J. Tang, “Glm: General language model pretraining with autoregressive blank infilling,” *arXiv preprint arXiv:2103.10360*, 2021.
- [20] H. Touvron, L. Martin, K. Stone, P. Albert, A. Almahairi, Y. Babaei, N. Bashlykov, S. Batra, P. Bhargava, S. Bhosale *et al.*, “Llama 2: Open foundation and fine-tuned chat models,” *arXiv preprint arXiv:2307.09288*, 2023.
- [21] M. Huang, J. Luo, C. Ding, Z. Wei, S. Huang, and H. Yu, “An integer-only and group-vector systolic accelerator for efficiently mapping vision transformer on edge,” *IEEE Transactions on Circuits and Systems I: Regular Papers*, 2023.
- [22] E. Kalali and R. Van Leuken, “Near-precise parameter approximation for multiple multiplications on a single dsp block,” *IEEE Transactions on Computers*, vol. 71, no. 9, pp. 2036–2047, 2021.
- [23] M. Huang, Y. Liu, S. Huang, K. Li, Q. Wu, and H. Yu, “Multi-bit-width cnn accelerator with systolic-in-systolic dataflow and single dsp multiple multiplication scheme,” in *Proceedings of the 2023 ACM/SIGDA International Symposium on Field Programmable Gate Arrays*, 2023, pp. 229–229.
- [24] P. Xue, L. Pan, L. Sun, and M. Huang, “Dual-line-systolic array for high performance cnn accelerator,” in *2022 IEEE 30th Annual International Symposium on Field-Programmable Custom Computing Machines (FCCM)*. IEEE, 2022, pp. 1–1.
- [25] S. Zeng, J. Liu, G. Dai, X. Yang, T. Fu, H. Wang, W. Ma, H. Sun, S. Li, Z. Huang *et al.*, “Flightllm: Efficient large language model inference with a complete mapping flow on fpgas,” in *Proceedings of the 2024 ACM/SIGDA International Symposium on Field Programmable Gate Arrays*, 2024, pp. 223–234.
- [26] Y. Huang, Y. Bai, Z. Zhu, J. Zhang, J. Zhang, T. Su, J. Liu, C. Lv, Y. Zhang, J. Lei, Y. Fu, M. Sun, and J. He, “C-eval: A multi-level multi-discipline chinese evaluation suite for foundation models,” in *Advances in Neural Information Processing Systems*, 2023.
- [27] C. Raffel, N. Shazeer, A. Roberts, K. Lee, S. Narang, M. Matena, Y. Zhou, W. Li, and P. J. Liu, “Exploring the limits of transfer learning with a unified text-to-text transformer,” *arXiv e-prints*, 2019.